Effects of Droplet-Wall Distance on Shock Wave Interaction with a Diesel Fuel Droplet under Conditions Related to Dual Fuel Internal Combustion Engines

Yu Jiao*[1], Steffen J. Schmidt[1], Nikolaus A. Adams[1]
[1]Chair of Aerodynamics and Fluid Mechanics, School of Engineering and Design, Technische Universität München, Boltzmannstr. 15, Garching bei München 85748, Germany
*Corresponding author: yu.jiao@tum.de

Abstract
In this investigation we study shock interaction of a diesel fuel droplet with diameter D in a mixed gas ambient in the vicinity to a wall (initial droplet distance H varies between H=0.5D to H=25D). The conditions are similar to single fuel (SF) ECN Spray A [1] chamber conditions and related to dual fuel internal combustion engines (DFICE). We apply a fully conservative multi-component numerical algorithm with interface sharpening combined with "Stiffened-Gas" EOS [2] and compute the diesel-droplet fragmentation process due to shock-droplet interaction. Our approach has been validated against reference data and shows excellent agreement. While processes like primary shock impingement, droplet deformation and droplet break-up are widely discussed in the literature [3-5], our focus is to include the effects of a reflected secondary shock (re-shock) due to the vicinity of a solid wall below the droplet. The re-shock reduces the mixture gas velocity in the main flow direction while it amplifies Richtmyer-Meshkov instibility (RMI). Depending on the initial distance between droplet and wall, various intermediate situations (PCS-situation, PSU-situation, PSC-situation) for droplet fragmentation are generated and discussed, which adds knowledge in spray and combustion processes in the DFICE environment.

Keywords
Shock-droplet interaction, Fully compressible flow, Dual fuel internal combustion engine, Diffuse interface method, Droplet fragmentation.

Introduction

Shock interaction with a two-phase interface has already been investigated by Richtmyer R. D. [6] and Meshkov E. E. [7]. The induced RMI is crucial for fuel mixing processes in internal combustion engines. In RMI related studies, processes like primary shock impingement, droplet deformation and droplet break-up are widely discussed in the literature [3-5, 9-11]. Duke-Walker [8] studied the effects of evaporation and break-up of droplets in the mixing induced by the shock-driven multiphase instabilities. Meng et al. [12] studied shock wave interaction with a water droplet and detailed structures were validated against experiments including chaotic flow features in the wake region caused by an instability growth. Kaiser et al. [13] numerically investigated a water droplet break-up induced by shock impingement and its resulting interface deformation. Sharma [14] obtained a criterion for the shifting process between the shear-induced entrainment mode and the Rayleigh-Taylor piercing mode during droplet break-up. However, re-shock effects were mostly not taken into account.

The re-shock promotes a secondary interaction with the two-phase interface and produces additional vorticity as well as altered pressure and velocity field characteristics. Haehn [15,16] experimentally studied the re-shock interaction with a bubble, where a re-shock reflected from the wall traversed the vortex ring and introduced additional vorticity. Leinov [19] studied shock and re-shock effects on RMI-induced mixing. Si [20] experimentally studied re-shock

helium and SF_6 bubbles in air at several bubble-wall distances. The initial distance between the bubble or the droplet towards the wall has strong effects on the re-shock shape and the resulting droplet fragmentation [17-20]. To our knowledge, the effects of both the primary shock and the re-shock resulting from the rear wall on a n-dodecane droplet in dual fuel conditions (mixed CH_4 and Air) are firstly studied in this investigation.

Numerical model and numerical methods

We extend and improve an existing fully compressible one-fluid model, which is part of our in-house solver CATUM. The vector of conserved quantities $\mathrm{q} = (\rho, \rho u, \rho v, \rho E, \rho \xi)$ is computed from the compressible Euler equations, $\partial q/\partial t + \nabla \cdot F_i(q) = 0$, as heat transfer, gravity, surface tension and viscous effects can be neglected due to the extremely short interface interaction time. Since a full thermodynamic model is used, baroclinic effects are taken into account. Higher order reconstruction is achieved by Minmod [24] and Koren [25] limiters used for density and velocity, respectively. The numerical reconstruction of internal energy follows the one for density. The algebraic compression method is used to reduce the smearing tendency of two-phase interfaces. A detailed description of the numerical methodology is under preparation.

We focus on the RMI induced by both, the primary shock and the resulting re-shock with a droplet in a dual fuel ambient. The dual fuel ambient is modeled by an ideal gas mixture and phase change processes are neglected. In our upcoming work an extension to real-fluid thermodynamic relations (table) will be presented.

Here, we use the “stiffened Gas” EOS for the liquid and both gas components

$$\mathrm{e}_\xi(\mathrm{P}_\xi, \rho_\xi) = \frac{\mathrm{P}_\xi + \gamma_\xi \mathrm{P}_{\infty,\xi}}{(\gamma_\xi - 1)\rho_\xi} + \mathrm{q}_\xi \tag{1}$$

$$\mathrm{c}_\xi{}^2 = \frac{\gamma_\xi(\mathrm{P}_\xi + \mathrm{P}_{\infty,\xi})}{\rho_\xi} \tag{2}$$

$$\rho_\xi(\mathrm{P}_\xi, \mathrm{T}_\xi) = \frac{\mathrm{P}_\xi + \mathrm{P}_{\infty,\xi}}{(\gamma_\xi - 1)\mathrm{C}_{\mathrm{V},\xi}\mathrm{T}_\xi} \tag{3}$$

In this investigation the gas reduces to ideal gas with $\mathrm{P}_{\infty,\mathrm{gas}} = 0$, $\mathrm{q}_{\mathrm{Gas}} = 0$ and $\mathrm{e}_{\mathrm{Gas}} = \mathrm{C}_{\mathrm{V,Gas}}\mathrm{T}_{\mathrm{Gas}}$

$$\mathrm{P}_{\mathrm{Gas}} = (\gamma_{\mathrm{Gas}} - 1)\rho_{\mathrm{Gas}}\mathrm{e}_{\mathrm{Gas}} = (\gamma_{\mathrm{Gas}} - 1)\rho_{\mathrm{Gas}}\mathrm{C}_{\mathrm{V,Gas}}\mathrm{T}_{\mathrm{Gas}} = \rho_{\mathrm{Gas}}\mathrm{R}_{\mathrm{Gas}}\mathrm{T}_{\mathrm{Gas}} \tag{4}$$

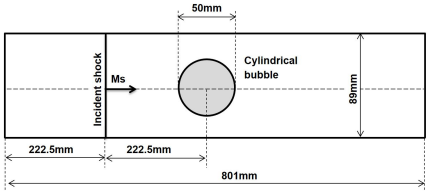

Figure 1. The schematic of shock-bubble interaction computational domain (sketch map).

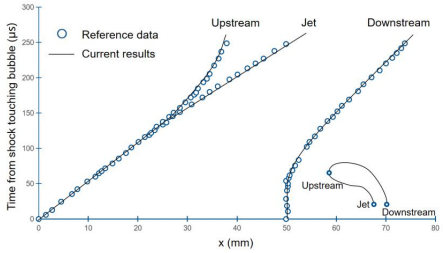

Figure 2. Space-time diagram for three characteristic two-phase interface points in the shock-bubble problem, comparing with results from Quirk and Karni [21].

Validation

We validate our numerical scheme with a shock-helium bubble case discussed in [21,22]. The computational domain is shown in Fig.1. The non-dimensional initial conditions are according to [22]: p=1, u=0, v=0, ρ =1 for pre-shocked air, p=1.5698, u=-0.394, v=0, ρ =1.3764 for post-shocked air, and p=1, u=0, v=0, ρ =0.138 for the helium bubble. A Cartesian mesh with uniform resolution of 0.5 mm is applied, see Fig.1. As depicted in Fig.2, the evolution history of three characteristic two-phase interface points are in excellent agreement with Quirk and Karni [21].

Results and Discussion

The schematic of the computational domain for the simulation of a shock-droplet interaction is shown in Fig.3. In the following, the distance H between the droplet and the rear wall varies from 0.5D to 25D, where D=10mm. An inviscid wall boundary condition is applied at the rear wall and non-reflective boundary conditions are applied elsewhere. Liquid diesel (n-dodecane) and a gas mixture (20% CH_4 and 80% Air) are represented by stiffened gas relations. For n-dodecane, we adopt the same thermodynamic parameters from reference [23], where $\gamma = 2.19, \mathrm{P}_\infty = 4 \times 10^8 \mathrm{Pa}, \mathrm{q} = -755 \times 10^3 \mathrm{J/kg}, \mathrm{C_V} = 1077 \mathrm{J/kg/K}$. The Mach number of the shock wave is set to around 1.23, which is nearly equal to the shock mach number of the classical air-helium shock-bubble interaction problem [21,22]. In this way, we adopt the following initial conditions accordingly:

For Pre-shocked mixed gas, $(\mathrm{p}, \mathrm{T}, \rho, \mathrm{c}) = (6000000[\mathrm{Pa}], 900[\mathrm{K}], 20.006[\mathrm{kg/m^3}], 656.397[\mathrm{m/s}])$, for Post-shocked mixed gas, $(\mathrm{p}, \mathrm{T}, \rho, \mathrm{c}) = (9096000[\mathrm{Pa}], 900[\mathrm{K}], 30.328[\mathrm{kg/m^3}], 656.397[\mathrm{m/s}])$, for Diesel droplet (liquid n-dodecane) [23], $(\mathrm{p}, \mathrm{T}, \rho, \mathrm{c}) = (6000000[\mathrm{Pa}], 363[\mathrm{K}], 872.683[\mathrm{kg/m^3}], 1009.385[\mathrm{m/s}])$.

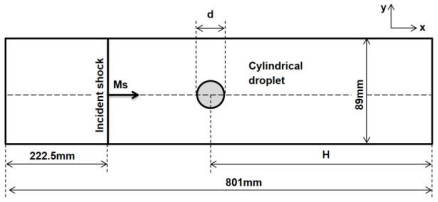

Figure 3. The schematic of shock-droplet interaction computational domain (sketch map).

Table 1. Effects of initial droplet-end wall distance on the shock-droplet and re-shock-droplet interaction characteristics.

Situation	1st interaction	2nd interaction	3rd interaction	Cases (H/D)
PCS	Primary shock	Contact wave	Secondary shock	20, 25
PSU	Primary shock	SUperimposed shock/contact region		17.5
PSC	Primary shock	Secondary shock	Contact wave	0.5, 5, 10, 15

We consider three situations as summarized in table 1. The situations differ by the interaction time of the droplet with the primary shock “P”, the contact wave “C” and the re-shock or secondary shock “S”. “SU” stands for the mixed superimposed shock/contact region. Depending on the situation, RMI and Kelvin-Helmholtz instability (KHI) have different growth properties and lead to different droplet break-up processes. In the following, we present representative cases for all three situations.

- **PCS-situation, taking H=20D for example.**

The distance in case H=20D is large enough to separately observe the effects of both, the primary and the secondary shock on the droplet fragmentation process. As shown in Fig.4 and Fig.6, the primary shock induces the initial RMI (Fig.4(a)) and the droplet breaks up (Fig.4(m)). Afterwards, the reflected secondary shock moves upstream and adds RMI to the fragments of the droplet causing further break-up of the mushroom structure into smaller ligaments (Fig.6(d)~(i)). In this situation, both shock waves have enough time to affect the two-phase interface independently. The RMI and the KHI have sufficient time to grow and develop.

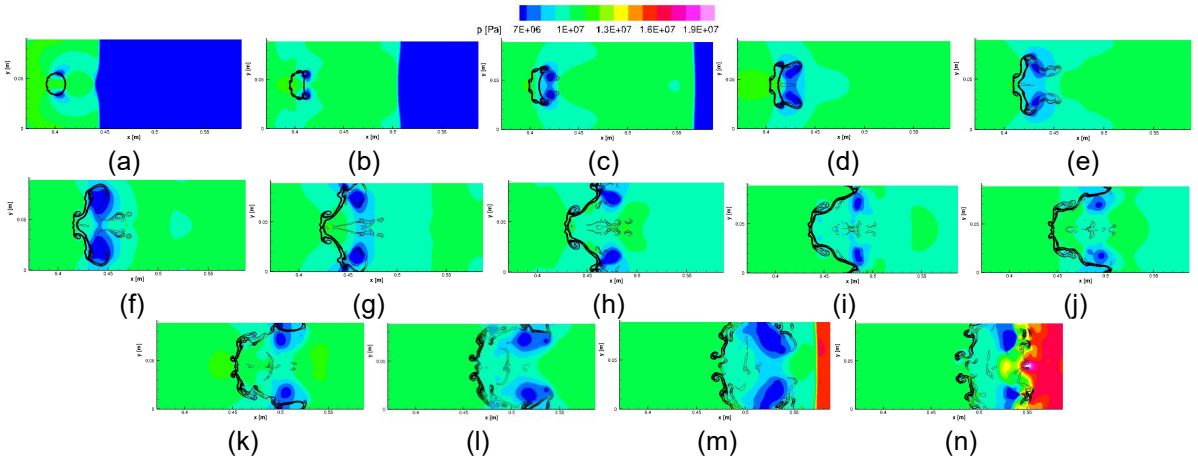

Figure 4. Evolution of pressure field and volume of fraction of mixed gas field.

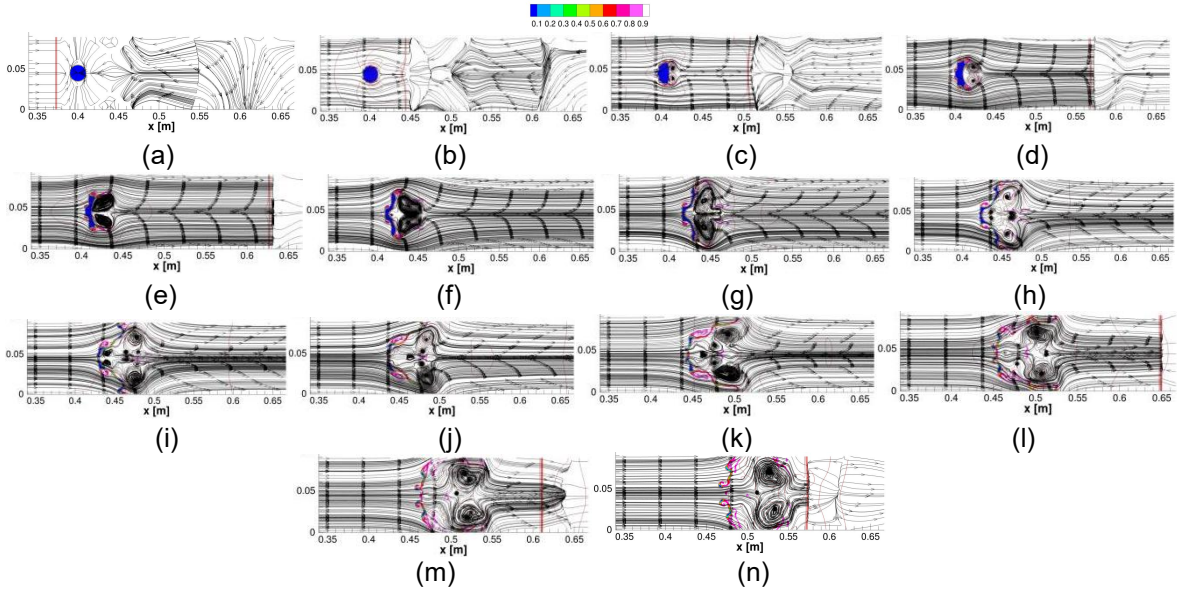

Figure 5. Evolution of streamline, wave and volume of fraction.

a. Primary shock-diesel droplet interaction in dual fuel environment.

In Fig.4 and Fig.5, the primary shock hits the droplet, which causes the initial RMI of droplet-gas interface (Fig.4(a), Fig5(b)). The counter rotating vortex pair (Fig.5(c)~(f)) appears after the primary shock passed the droplet. The droplet is elongated in stream-wise direction and widens in normal direction (Fig.4(a)~(c),Fig.5(b)~(d)). The inertia of the shocked gas mixture enhances the growth of RMI and KHI (Fig5(c)~(f)) and the droplet gradually breaks up (Fig.4(l)~(n), Fig.5(m)~(n)).

b. Secondary re-shock diesel droplet interaction in dual fuel environment.

In this process, the droplet has already broken into parts before the re-shock reaches the droplet region (Fig6(a)~(b), Fig7(a)). As shown in Fig.6, the secondary re-shock firstly

interacts with the downstream edge of the droplet ligaments (Fig.6(b), Fig7(a)) and then lengthens the mushroom head in upstream direction (Fig.6(e), Fig7(d)). The re-shock reduces the velocity of the gas mixture in the main flow direction, interacts with the fragmented droplet and adds additional RMI, which results in further break-up of separated ligaments (Fig6(e)~(i), Fig7(d)~(h)). As the re-shock further promotes the fragmentation in the break-up process, it could be useful in enhancing dual fluid mixing processes of DFICE.
In Fig.7, the re-shock causes additional vorticity and changes the vortex distribution characteristics (Fig.7(c)~(d)). The resulting vortex pair rotates in opposite direction to the original one, which further increases disturbances and enhances fluid mixing in the fragmentation region (Fig.7(h)).

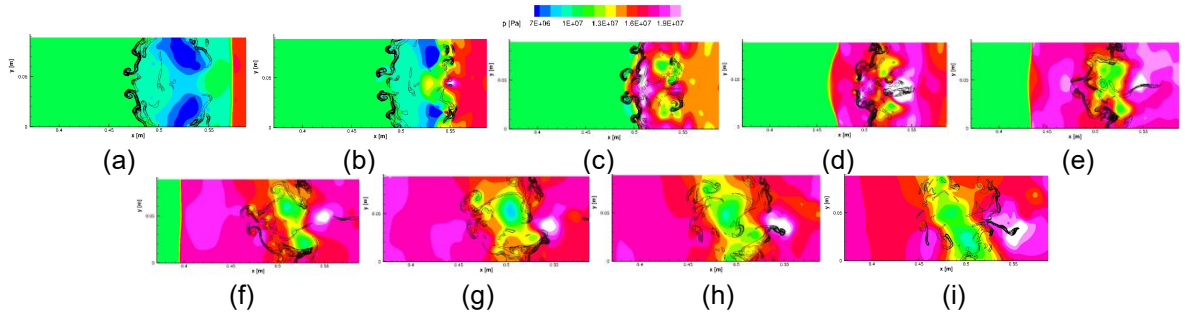

Figure 6. Evolution of pressure field and volume of fraction field.

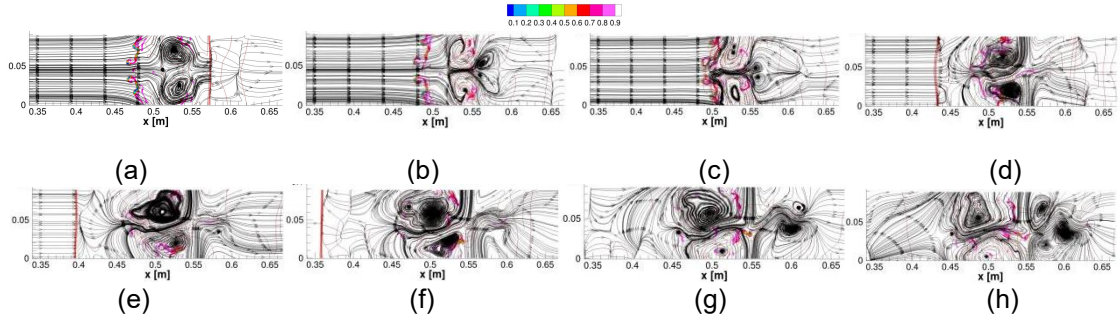

Figure 7. Evolution of streamline, wave and volume of fraction.

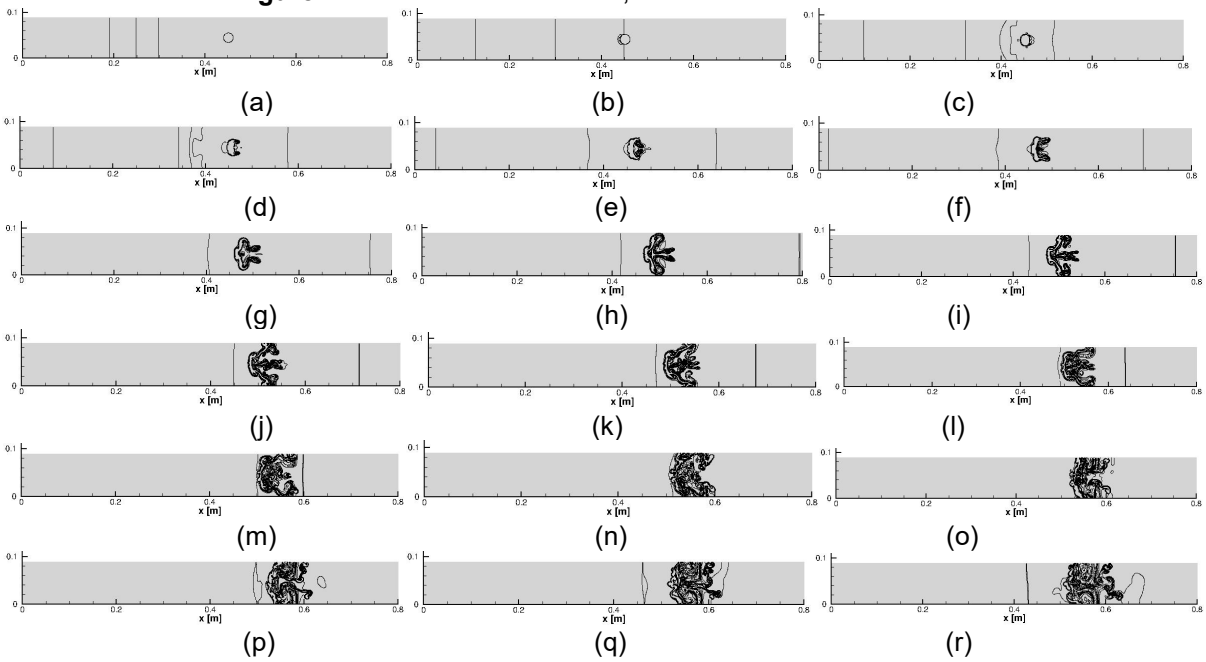

Figure 8. Evolution of shock wave.

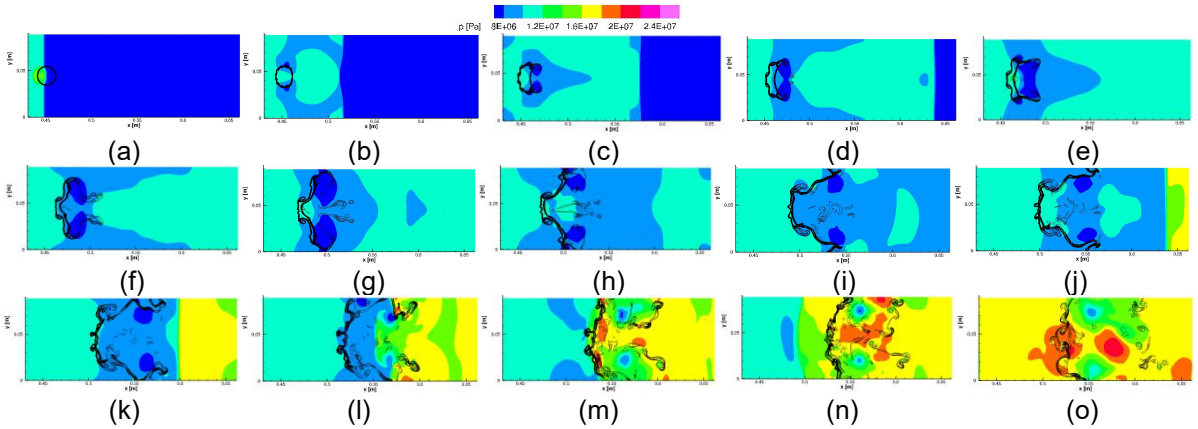

Figure 9. Evolution of volume of fraction field.

• **PSU-situation, taking H=17.5D for example.**

Here, the re-shock meets with the contact wave in the fragmentation region (Fig.8(m)~(o), Fig.9(k)~(m)). The initial RMI and induced KHI have not enough time to split the droplet into parts before the re-shock approaches the fragmentation region. As shown in Fig.8(m) and in Fig.9(l), the mushroom shape grows towards the upstream direction, followed by enhanced mixing and break-up into small ligaments (Fig.8.(q)~(r),Fig.9(o)). The fragmentation is less pronounced than in PCS situation.

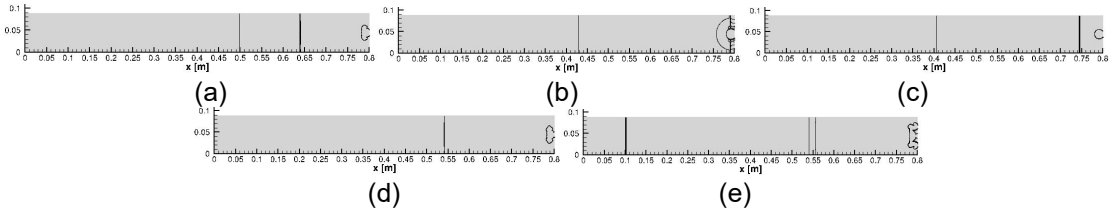

Figure 10. Evolution of shock wave.

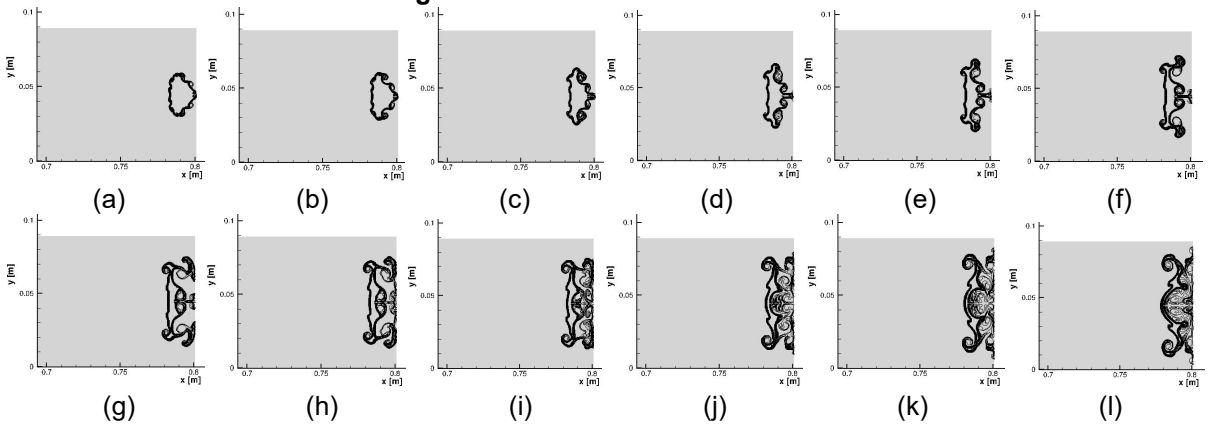

Figure 11. Evolution of volume of fraction field.

• **PSC-situation, taking H=0.5D for example.**

In this situation, the shock-droplet interaction time between the primary and the secondary shock is short, so that the two-phase instabilities (RMI, KHI) have limited time to develop and grow before the re-shock reaches the droplet. The contact wave slows down due to the re-shock and does not reach the droplet fragmentation region (Fig.10(d)~(e)). As shown in Fig.10, the primary shock firstly reaches the droplet region (Fig.10(b)) and then reflects back (Fig.10(c)), and encounters the contact wave (Fig.10(d)). The contact wave slows down

(Fig.10(e)) and the structures in Fig.11 are purely due to the effects of primary shock and re-shock. Fig.11 shows the evolution of shock induced RMI in upstream and in normal direction The mushroom jets in normal direction (Fig.11(f)~(i)) impact on the wall due to the selected set-up.

Conclusions

In this investigation, we focus on primary shock and re-shock interactions with a diesel droplet at different droplet-wall distances. The distance affects the RMI growth and droplet fragmentation and determines time intervals of wave interaction on the droplet. Depending on dominating droplet-wave interaction processes, we define three typical situations called PCS-situation, PSU-situation and PSC-situation and analyze their specific characteristics.

PCS-situations provide enough time for the initial RMI to grow and for KHI to develop near the two-phase interface, which breaks up the droplet and enhance fluid mixing performance. The PSU-situation limits the development process of initial RMI and KHI as two kinds of wave meet with each other in the droplet fragmentation region, thus delaying the break-up process due to opposite wave motion. In PSC-situations the close vicinity of the wall blocks the break-up process of droplet ligaments. The development of RMI and KHI is suppressed due to a very short intermediate time interval between shock and re-shock. For a very short droplet-wall distance, the instability-induced downstream mushroom may impact at the wall and the mushroom structures reflected from the wall could further enhance the growth of upstream mushroom structures. However, droplet splash phenomena and resulting upstream mushroom structures require further three-dimensional studies with higher spatial resolution.

We suppose that this work provides information hints on how a primary and a reflected shock could enhance the break-up and the mixing process in engineering applications of DFICE. Further work will contain enhanced real-fluid thermodynamic relations (table) and detailed three-dimensional simulations over a large Mach number range including additional physical effects.

Acknowledgments

This research was supported by the EDEM project. This project has received funding from the European Union Horizon 2020 Research and Innovation programme under Grant Agreement No 861002. The authors also gratefully acknowledge the Leibniz Supercomputing Centre for funding this research by providing computing time on its Linux-Cluster.

References

[1] Engine Combustion Network, https://ecn.sandia.gov/diesel-spray-combustion/target-condition/spray-ab/.

[2] Harlow, F. H., & Amsden, A. A.,1971, Fluid Dynamics. A LASL Monograph (No. LA-4700). Los Alamos National Lab.(LANL), Los Alamos, NM (United States).

[3] Quirk, J., & Karni, S., 1996, On the dynamics of a shock–bubble interaction. Journal of Fluid Mechanics, 318, pp129-163.

[4] Ranjan, D., Oakley, J., & Bonazza, R., 2011, Shock-bubble interactions. Annual Review of Fluid Mechanics, 43, pp117-140.

[5] Delale, Can F., 2013, “Bubble Dynamics and Shock Waves”, Springer Berlin Heidelberg.

[6] Richtmyer R D., 1960, Taylor instability in shock acceleration of compressible fluids. Comm Pure Appl Math, 13: pp297–319.

[7] Meshkov E E., 1972, Instability of the interface of two gases accelerated by a shock wave. Fluid Dyn, 4: pp101–104.
[8] Duke-Walker, Vasco; Maxon, W. Curtis; Almuhna, Sahir R.; McFarland, Jacob A., 2021, Evaporation and breakup effects in the shock-driven multiphase instability. In J. Fluid Mech. 908.
[9] Theofanous, T., 2011. Aerobreakup of Newtonian and viscoelastic liquids. Annu. Rev. Fluid Mech. 43 (1), pp661–690.
[10] Zabusky N J., 1999, Vortex paradigm for accelerated inhomogeneous flows: Visiometrics for the Rayleigh-Taylor and Richtmyer-Meshkov environments. Annu Rev Fluid Mech, 31: pp495-536.
[11] Brouillette M., 2002, The Richtmyer-Meshkov instability. Annu Rev Fluid Mech, 34: pp445-468.
[12] Meng, Jomela C.; Colonius, Tim, 2018, Numerical simulation of the aerobreakup of a water droplet. In J. Fluid Mech. 835, pp. 1108-1135.
[13] Kaiser, J.W.J.; Winter, J. M.; Adami, S.; Adams, N. A., 2020, Investigation of interface deformation dynamics during high-Weber number cylindrical droplet breakup. In International Journal of Multiphase Flow 132, p. 103409.
[14] Sharma, S., Singh, A. P., Rao, S. S., Kumar, A., & Basu, S., 2021, Shock induced aerobreakup of a droplet. Journal of Fluid Mechanics, 929.
[15] Haehn, N.; Weber, C.; Oakley, J.; Anderson, M.; RANJAN, D.; BONAZZA, R., 2011, Experimental investigation of a twice-shocked spherical gas inhomogeneity with particle image velocimetry. In Shock Waves 21 (3), pp. 225-231.
[16] Haehn, N.; Weber, C.; Oakley, J.; Anderson, M.; RANJAN, D.; BONAZZA, R., 2012, Experimental study of the shock-bubble interaction with re-shock. In Shock Waves 22 (1), pp. 47-56.
[17] Brouillette M, Sturtevant B., 1994, Experiments on the Richtmyer-Meshkov instability: Single-scale perturbations on a continuous interface. J Fluid Mech, 263: 271-292.
[18] Houas L, Chemouni I., 1996, Experimental investigation of Richtmyer-Meshkov instability in shock tube. Phys Fluids, 8: pp614-627.
[19] Leinov E, Malamud G, Elbaz Y, et al. 2009, Experimental and numerical investigation of the Richtmyer-Meshkov instability under re-shock conditions. J Fluid Mech, 626: 449-475.
[20] Si, Ting; Zhai, Zhigang; Yang, Jiming; Luo, Xisheng, 2012, Experimental investigation of re-shocked spherical gas interfaces. In Phys. Fluids 24 (5), p. 54101.
[21] Quirk, J., & Karni, S., 1996, On the dynamics of a shock-bubble interaction. Journal of Fluid Mechanics, 318, pp129-163.
[22] Fedkiw, Ronald P.; Aslam, Tariq; Merriman, Barry; Osher, Stanley, 1999, A Non-oscillatory Eulerian Approach to Interfaces in Multimaterial Flows (the Ghost Fluid Method). In Journal of Computational Physics 152 (2), pp. 457-492.
[23] Le Métayer, O., Massoni, J., & Saurel, R., 2005, Modelling evaporation fronts with reactive Riemann solvers. Journal of Computational Physics, 205(2), pp567-610.
[24] P. L. Roe, Characteristic-based schemes for the Euler equations, Annu Rev Fluid Mech 18 (1986) 337–365.
[25] B. Koren, A robust upwind discretization method for advection, diffusion and source terms, in: Koren Vreugdenhil (Ed.), Numerical Methods forAdvection–Diffusion Problems, Vieweg, Braunschweig, Germany, 1993, pp. 117–138.